XLI CILAMCE
XLI Ibero-Latin American Congress on Computational Methods in Engineering
16-19 November, 2020 FOZ DO IGUAÇU PARANÁ - BRAZIL

# Geometrically nonlinear buckling analysis of cement-based structures with thermoelastic effects and material damage

Henrique C. F. Curci[1], Eduardo M. B. Campello[1], Henrique C. Gomes[1]

[1] *Dept. of Structural and Geotechnical Engineering, University of São Paulo, Brazil*
*henrique.curci@usp.br, campello@usp.br, henrique.campelo@usp.br*

**Abstract.** This work presents a geometrically nonlinear formulation for the analysis of buckling problems involving cement-based structures susceptible to thermoelastic effects and progressive material damage. Particularly, we are interested in simulating bifurcation and snap-through phenomena of columns and shallow arches under such conditions. The thermoelastic material implementation is based on a multiplicative decomposition of the deformation gradient, wherein the temperature field is assumed to be known (given). Damage effects, in turn, are taken into account based on a simple (yet representative) nonlocal continuum damage mechanics (CDM) model, namely, the Mazars' scalar model, the nonlocality of which is ensured by means of a homogenization of the elastic equivalent deformation field. The formulation is implemented in an in-house finite element code developed by the authors including tools for solving two-dimensional plane strain problems. The model is solved within an iterative, fully consistent Newton-Raphson scheme. A numerical example is provided to validate our model and illustrate its capabilities against known results from the literature.

**Keywords:** Stability analysis, geometrical nonlinearities, damage, thermal effects, concrete structures

## 1 Introduction

Slender structures are susceptible to instability problems (such as buckling) due to geometrical and/or material nonlinearities related to softening processes, which may be induced, e.g., by damage evolution in cement-based concrete structures. Evaluation of damage in cement-based structures and its representation within numerical modelling is usually marked by some challenging implementational aspects. As the damage from stiffness degeneration induces a strain-softening behavior, it is common to face strain-localization issues, despite the simplicity that is offered by an isotropic local damage function approach. As commented by Belytschko et al. [1], finite element solutions based on such approach usually exhibit dependence on mesh element size, and increasing the level of mesh refinement does not help as problems in energy dissipation in such localization zones may occur, thereby affecting the solution´s convergence. Whithin the continuum damage mechanics (CDM) approach, in which the definition of a representative volume element (RVE) is critical to properly perform local homogenization, the consideration of a nonlocal damage model, as proposed by many authors (see Bažant [2] and Pijaudier-Cabot [3], for example), is a valid approach to avoid such difficulties from material softening.

This work presents a geometrically nonlinear formulation for the analysis of buckling problems involving cement-based structures susceptible to thermoelastic effects and progressive material damage. We follow the nonlocal approach. We are interested here in the analysis of plane strain slabs and columns subjected to thermal strains. The thermoelastic problem is based on a multiplicative decomposition of the deformation gradient, wherein the temperature field is assumed to be known. Damage effects, in turn, are taken into account based on a simple (yet representative) nonlocal continuum damage mechanics model, namely, the Mazars' scalar model, the nonlocality of which is ensured by means of a homogenization of the elastic equivalent deformation field. The formulation is implemented in an in-house finite element code developed by the authors including tools for solving two-dimensional plane strain problems. The model is solved within an iterative Newton-Raphson. This work is a

continuation of a former work by some of the authors presented in [4]. The paper is organized as follows. In sections 2 to 4 we present our formulation (kinematics, damage, numerical problem and its corresponding solution scheme, respectively) and some implementation aspects. In section 5 we present a numerical application, including a brief discussion on the results and also the advantages and disadvantages regarding different solver methods. In section 6 we close the paper with our conclusions and final considerations. Throughout the text, plain italic letters ($a, b, \ldots, A, B, \ldots$) denote scalar quantities; boldface lowercase italic letters ($\boldsymbol{a}, \boldsymbol{b}, \ldots, \boldsymbol{a}, \boldsymbol{b}, \ldots$) denote vectors; and boldface capital italic letters ($\boldsymbol{A}, \boldsymbol{B}, \ldots$) denote second-order tensors in a three-dimensional Euclidean space. The inner product of two vectors is denoted by $\boldsymbol{u} \times \boldsymbol{v}$, and the norm of a vector by $\|\boldsymbol{u}\| = \sqrt{\boldsymbol{u} \times \boldsymbol{u}}$.

# 2 Formulation and numerical solution scheme

Although cement-based materials damage analysis is usually associated to small strains, the formulation to be presented here includes geometrical nonlinear effects in order to adequately capture instability phenomena. We adopt a (damageable) hyperelastic material representation for the elastic part of the deformation. The formulation is introduced for two-dimensional plane strain problems from the outset. Both the constitutive representation and the nonlocal damage formulation are preceded by a Lagrangian kinematic description of an arbitrary thermoelastic transformation, in which large displacements and deformations are fully permitted.

## 2.1 Kinematics and equilibrium

Consider a two-dimensional representation of a body that occupies a region $\Omega$ and has a contour $\Gamma$ in the Euclidean space (based in a global orthonormal reference base $\boldsymbol{e}_i$) at any time. If the superscripted "$r$" (as in $\blacksquare^r$) is adopted to designate any parameter or body property in the reference configuration (related to a region $\Omega^r$ with mass density $\rho_r$), any point belonging to this body in this configuration can be described by its position vector $\boldsymbol{x}^r$, or else by $\boldsymbol{x}$ in the current configuration. The transformation generates a displacement field $\boldsymbol{u} = \boldsymbol{x} - \boldsymbol{x}^r$, as shown in Fig. 2. The total deformation gradient $\boldsymbol{F}$ and the displacement gradient $\boldsymbol{L}$ are given by

$$\boldsymbol{F} = \nabla \boldsymbol{x} = \frac{\partial \boldsymbol{x}}{\partial \boldsymbol{x}^r} = \boldsymbol{f}_i \otimes \boldsymbol{e}_i = [\boldsymbol{f}_1 \; \boldsymbol{f}_2 \; \boldsymbol{e}_3] \quad \textit{and} \quad \boldsymbol{L} = \nabla \boldsymbol{u} = \frac{\partial \boldsymbol{u}}{\partial \boldsymbol{x}^r} = \boldsymbol{\gamma}_i \otimes \boldsymbol{e}_i = [\boldsymbol{\gamma}_1 \; \boldsymbol{\gamma}_2 \; \boldsymbol{0}], \tag{1}$$

where $\otimes$ is the (standard) tensor product. We use here a reduced notation based on column-vectors $\boldsymbol{f}_i$ and $\boldsymbol{\gamma}_i$, and note that the plane-strain particularization is already introduced since $\boldsymbol{f}_3 = \boldsymbol{e}_3$ and $\boldsymbol{\gamma}_3 = \boldsymbol{0}$. Tensor $\boldsymbol{F}$ represents both the elastic-damage and the thermal transformations. The thermal-related deformation gradient $\boldsymbol{F}_\theta$ is taken here as linearly dependent of the temperature field $\theta$ and is given through (see Lu and Pister [5])

$$\boldsymbol{F}_\theta = \bar{v}(\theta)\boldsymbol{I} = (1 + \alpha \Delta\theta)\boldsymbol{I} = v\boldsymbol{I}, \tag{2}$$

where $\Delta\theta = \theta - \theta^r$ is the thermal variation around a reference temperature $\theta^r$ (intended to be the temperature field related to a stress-free initial state) and $\alpha$ is the material´s thermal expansion coefficient. As it can be seen, this volumetric transformation is assumed to be fully isotropic.

For arbitrarily large deformations, some strategy must be considered to split the total deformation gradient into its thermal and elastic counterparts in a consistent way. The multiplicative decomposition to be used here was proposed firstly by Micunovic [6] and is largely used by other authors (see, e.g., Vujošević and Lubarda [7]). This approach allows the partition of the total deformation gradient as

$$\boldsymbol{F} = \boldsymbol{F}_e \boldsymbol{F}_\theta, \text{ with } \boldsymbol{F}_e = \boldsymbol{f}_{ei} \otimes \boldsymbol{e}_i. \tag{3}$$

This approach is also used in finite-strain elastoplastic transformations (see, e.g., Campello [8], Campello et al. [9]). The multiplicative decomposition approach also demands the total transformation partition in an intermediate stage, characterized by stress-free thermal deformations without any strain restrictions. Figure 1(b) addresses this intermediate transformation and shows each configuration particularities. Considering that both damage evolution process and constitutive relation take place within the purely elastic part of the transformation, is important to obtain and evaluate the elastic deformation gradient in terms of total and thermal deformations. Due to the simplicity of $\boldsymbol{F}_\theta$ (as an invertible matrix), it is easy to express $\boldsymbol{F}_e$ and $J_e$ as

$$\boldsymbol{F}_e = \upsilon^{-1}\boldsymbol{F} \text{ (with } \boldsymbol{f}_{ei} = \upsilon^{-1}\boldsymbol{f}_i) \text{ and } J_e = det\,(\boldsymbol{F}_e) = \upsilon^{-3}J. \tag{4}$$

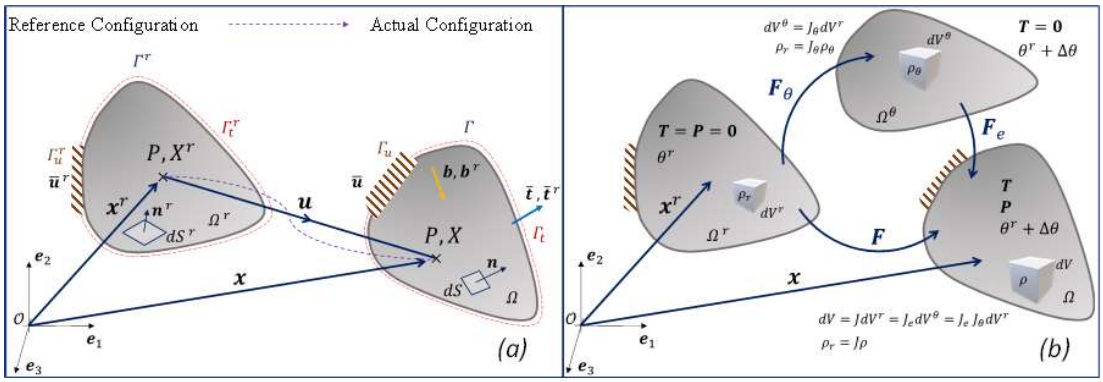


Figure 1. (a) Deformable solid under arbitrary (nonlinear) transformation. (b) Transformation based on multiplicative decomposition: fictitious configuration representation

As seen in Figure 1(b), the purely elastic transformation $\boldsymbol{F}_e$ starts from an already deformed (though stress-free) configuration $\Omega^\theta$, which has mass density $\rho_\theta = \upsilon^{-3}\rho_r$ (due to expansion with mass conservation). For the static problem description in the reference configuration, the equilibrium and compatibility (related to boundary conditions) equations to be solved are

$$\begin{cases} div\,\boldsymbol{P} + \boldsymbol{b}^r = \boldsymbol{0} & in\ \Omega^r \\ \boldsymbol{u} = \overline{\boldsymbol{u}} & in\ \Gamma_u^r \\ \boldsymbol{t} = \overline{\boldsymbol{t}} & in\ \Gamma_t^r, \end{cases} \tag{5}$$

considering the mass forces $\boldsymbol{b}^r$ (per unit volume of the reference configuration) and the traction vector ($\boldsymbol{t}^r$) of a surface point (per unit area of the reference configuration), which is related to the 1st Piola-Kirchhoff (P-K) stress tensor and the normal vector $\boldsymbol{n}^r$ (in the reference configuration) in the point by $\boldsymbol{P}\boldsymbol{n}^r = \boldsymbol{t}^r$. Equation (5) is the boundary value problem to be to be solved subsequently through the principle of virtual work (PVW).

The proposed formulation must correctly represent the transformation regarding both thermoelastic and elastic-damage effects. Therefore, is important to observe it under the criterion of thermodynamic equilibrium (related to the dissipated internal energy equation). Considering a scalar isotropic damage parameter $d$ and a damageable hyperelastic specific Helmholtz free energy function $\psi_d = \hat{\psi}_d(\boldsymbol{F}_e, d)$ (independent of temperature) and the Clausius-Planck inequality written in the reference configuration, the internal dissipation energy $\mathcal{D}_{int}$ is (see [10])

$$\mathcal{D}_{int} = \boldsymbol{P}_e : \dot{\boldsymbol{F}}_e - \rho_r\left[\eta\dot{T} + \dot{\psi}_d\right] \geq 0 \qquad \text{with} \qquad \dot{\psi}_d = \frac{\partial\hat{\psi}_d(\boldsymbol{F}_e, d)}{\partial\boldsymbol{F}_e} : \dot{\boldsymbol{F}}_e + \frac{\partial\hat{\psi}_d(\boldsymbol{F}_e, d)}{\partial d}\dot{d}\,, \tag{6}$$

which is related to reversible (if $\dot{d} = 0$) or irreversible processes. Note that this approach is dependent of the hypothesis that $\mathcal{D}_{int}$ is not affected by the heat flux if $\dot{T} = 0$ (isothermal process), which can be valid for quasi-static uncoupled problems, so $\mathcal{D}_{int} = \boldsymbol{P}_e : \dot{\boldsymbol{F}}_e - \rho_r\dot{\psi}$. Furthermore, this formulation (with damage) proves to be appropriate for problems involving finite displacements but small deformations (as should be expected for cement-based materials behavior). If the damage function is built from the relationship between intact and damaged areas, both Helmholtz free energy function $\hat{\psi}_d(\boldsymbol{F}_e, d)$ and the energy release rate by the growth of microcracks ($Y$) are given by

$$\hat{\psi}_d(\boldsymbol{F}_e, d) = (1-d)\hat{\psi}_e(\boldsymbol{F}_e) \qquad and \qquad Y = \frac{\partial\hat{\psi}_d(\boldsymbol{F}_e, d)}{\partial d} = -\hat{\psi}_e(\boldsymbol{F}_e)\,. \tag{7}$$

The Clausius-Duhem inequality condition for the second law of thermodynamics is verified if $Y\dot{d} \geq 0$ and, as $Y$ must be positive, the scalar damage evolution must be crescent throughout the thermoelastic process.

### 2.2 Constitutive relation

The constitutive relation adopted here is based on the so-called Simo-Ciarlet hyperelastic material, which allows to represent a transformation for arbitrary finite displacements (requirement to properly capture the path in instability problems). The use of this relation has some advantages, as its simplicity (in consideration of the thermal parameters inclusion, also) provides a straightforward implementation. The correct derivation of the Simo-Ciarlet strain energy function $\psi_e(\boldsymbol{F}_e)$ allows us to obtain both the 1st P-K stress tensor (described by its column-vectors $\boldsymbol{\tau}_{ei}$) and the fourth-order tensor of elastic tangent moduli $\boldsymbol{K}_T$ (in which the second-order components $\boldsymbol{C}_{ij}$ are used to form the fourth-order tensor $\boldsymbol{K}_T$), to be used further below within the numerical schemes. Accordingly, the stresses $\boldsymbol{\tau}_{ei}$ and tensors $\boldsymbol{C}_{ij}$ are

$$\boldsymbol{\tau}_{ei} = (1-d)\left\{\upsilon^{-3}\left[\frac{\lambda}{2}\left({J_e}^2-1\right)-\mu\right]J_e^{-1}\boldsymbol{g}_{ei}+\upsilon^{-3}\mu\boldsymbol{f}_{ei}\right\} \quad \text{and} \tag{8}$$

$$\boldsymbol{C}_{ij} = (1-\mathrm{d})\{\bar{\phi}(J)\boldsymbol{g}_i\otimes\boldsymbol{g}_j+\left[\delta_{ij}.(\mu\boldsymbol{I}+\phi(J)skew(\boldsymbol{e}_3))-\phi(J)skew(\boldsymbol{e}_3)\right]\}, \quad \text{where} \tag{9}$$

$$\bar{\phi}(J)=\frac{\lambda}{2}(1+J^{-2})+\mu J^{-2} \quad \text{and} \quad \phi(J)=\frac{\lambda}{2}[(J^2-1)-\mu]J^{-1}\,. \tag{10}$$

In the above expressions, one has $\boldsymbol{g}_i=-\boldsymbol{f}_j\,skew(\boldsymbol{e}_3)$. For a detailed description, see Curci et al. [4], Wriggers [11] and Gomes [12]. This constitutive formulation allows us to solve the geometrically nonlinear problem with a fully quadratic convergence rate for purely elastic transformations. For the material nonlinearities induced by the nonlocal damage process, the stiffness matrix $\boldsymbol{K}_T$ is no longer tangent is no longer tangent, and the quadratic convergence is lost at some conditions (i.e., damage growth). The criteria for damage modelling are presented in the next section.

## 3 Damage modeling and nonlocal approach

The material softening behavior adopted here is the classical Mazars' damage model [13]. This model is well-known and usually applied for cement-based materials, due to its simplicity (as an isotropic and scalar model) and the capacity to represent the concrete brittle and quasi-brittle behavior with a function that evaluates the damage evolution through a combined failure mode I (tensile) and II (shear). From the consideration of the Helmholtz free energy Ψ state potential and the thermodynamics background, Mazars' damage model evaluates the growth of microcracks into concrete matrix starting from a yield surface function $f(\bar{\varepsilon},\mathcal{K}_d)$ (to be dependent of nonlocal equivalent strain, $\bar{\varepsilon}$). This function is presented as

$$f(\bar{\varepsilon},\mathcal{K}_d)=\bar{\varepsilon}-\mathcal{K}_d\leq 0, \tag{11}$$

in which $\mathcal{K}_d$ is a strain threshold for damage non-growth, classified as the maximum equivalent strain achieved in that point (and limited by a material-dependent initial threshold $\mathcal{K}_0$). For the sake of brevity, eq.(11) above is already presented with the yield surface as a function of this nonlocal equivalent strain, which depends on the spatial average of local equivalent strain $\tilde{\varepsilon}$ around the region to be analyzed. The main advantage of using a nonlocal approach to represent damage growth is to avoid problems with strain localization due to the softening process (see [14]). In addition, a nonlocal approach to deformations better represents mesoscale homogenization, considering a continuum damage on the representative volume element (RVE). The local equivalent strain $\tilde{\varepsilon}$ can be evaluated for a generic point as $\tilde{\varepsilon}=\|\langle\boldsymbol{\varepsilon}_i\rangle_+\|$, with $\langle\boldsymbol{\varepsilon}_i\rangle_+$ as a vector originated by the positive part of the eigenvalues $\varepsilon_i$ from the symmetric Green-Lagrange tensor $\boldsymbol{E}$, and $\langle\varepsilon_i\rangle_+$=$0.5(\varepsilon_i+|\varepsilon_i|)$. The nonlocal equivalent strain $\bar{\varepsilon}$ is then obtained through the following volume integration

$$\bar{\varepsilon}\,(\boldsymbol{x}^r)=\frac{1}{V(\boldsymbol{x}^r)}\int_{\Omega^r}\Phi(\boldsymbol{s}^r-\boldsymbol{x}^r).\,\tilde{\varepsilon}\,(\boldsymbol{s}^r)d\Omega^r \quad (with \quad V(\boldsymbol{x}^r)=\int_{\Omega^r}\Phi(\boldsymbol{s}^r-\boldsymbol{x}^r)d\Omega^r\,), \tag{12}$$

which represents a weighted spatial average of $\tilde{\varepsilon}$ in the domain $\Omega^r$, with $\Phi(\boldsymbol{s}^r-\boldsymbol{x}^r)$ as the weight function. This analysis is centered in the point with coordinates $\boldsymbol{x}^r$ and must scan both weight functions and local equivalent strains from points with coordinates $\boldsymbol{s}^r$ around the target point. The function Φ to be used here (see Bažant and

Pijaudier-Cabot [2]) is

$$\Phi(\boldsymbol{s}^r - \boldsymbol{x}^r) = exp[-(2.\|\boldsymbol{s}^r - \boldsymbol{x}^r\|.d_{lim}^{-1})^2], \tag{13}$$

which is exponential and decays to insignificant values for distances greater than $d_{lim}$, i.e., $\Phi$ must be evaluated only for $\|\boldsymbol{s}^r - \boldsymbol{x}^r\| \leq d_{lim}$. The parameter $d_{lim}$ is related to the RVE, on which the continuum media description is based. From this on, the damage is obtained through the ponderation of two exponential damage laws which comprises a tensile ($d_T$) and a compressive ($d_C$) part of the damage. These laws are functions of the curve fitting parameters ($A_C$, $A_T$, $B_C$ and $B_T$), the nonlocal equivalent strain $\bar{\varepsilon}$ and the initial strain threshold $\mathcal{K}_0$, as

$$d_T = \hat{F}_T(\bar{\varepsilon}) = 1 - [(1 - A_T)\mathcal{K}_0/\bar{\varepsilon}] - \left[A_T/exp\left(B_T(\bar{\varepsilon} - \mathcal{K}_0)\right)\right] \text{ and} \tag{14.1}$$

$$d_C = \hat{F}_C(\bar{\varepsilon}) = 1 - [(1 - A_C)\mathcal{K}_0/\bar{\varepsilon}] - \left[A_C/exp\left(B_C(\bar{\varepsilon} - \mathcal{K}_0)\right)\right]. \tag{14.2}$$

The weighting of $d_T$ and $d_C$ is achieved through a composition dependent on scalar coefficients $\alpha_T$ and $\alpha_C$ (respecting $\alpha_T + \alpha_C = 1$), the latter defined by the stress-strain state of the analyzed point. That way, it gives $d = \alpha_T.d_T + \alpha_C.d_C$. These coefficients are evaluated by calculating the positive and negative parts of strains related to the linearized stress partition (see Álvares [15]).

# 4 Numerical discretization and solver schemes

For the numerical solution, we resort to the standard Finite Element Method. The region $\Omega^r$ is discretized by quadratic, isoparametric, triangular elements (6 nodes) and the displacements field $\boldsymbol{u}(\boldsymbol{x}^r)$ is approximated by quadratic polynomial shape functions $\mathbf{N}$ (and their spatial derivatives $\mathbf{N}_{,i}$.). The nodal displacement vector $\boldsymbol{u_e}$ for each element is then used to evaluate the displacements at any point inside the element, and the displacement field vector $\mathbf{u}$ (related to the global d.o.f.s) is approximated by the union of those nodal displacements. Accordingly, applying the PVW on the boundary value problem of eq. (*5*), the objective is to solve, for a step $st$, the nonlinear unbalanced forces relation $\mathbf{R}^{st}$ from

$$\delta\boldsymbol{u}^T \int_{\Omega_e^r} (1-d)\boldsymbol{N}_{,i}^T\boldsymbol{\tau}_i \, d\Omega_e^r = \delta\boldsymbol{u}^T\boldsymbol{R}_{int} = \delta\boldsymbol{u}^T\lambda_f^{st}\boldsymbol{R}_{ext} \;\rightarrow\; \boldsymbol{R}^{st} = \lambda_f^{st}\boldsymbol{R}_{ext} - \boldsymbol{R}_{int} = \mathbf{0}, \tag{15}$$

in which $\lambda_f^{st}$ is the external forces control parameter for an incremental analysis. Considering the material nonlinearity induced by damage growth and softening, the standard Newton-Raphson method generally fails to encounter a solution after the problem reaches a limit point (related to the maximum external load or temperature that can be equilibrated by the elastic internal forces) due to the post-peak negative stiffness matrix. The numerical example to be explored here uses only the standard Newton-Raphson method, as the results with nonlocal approach presented good convergence for purely thermal loads. To consider only temperatures varying in the Newton-Raphson procedure, the expression (15) must be rewritten to consider the inexistence of external loads. In such case, the temperature increments by $\lambda_t^{st}$ (temperature control parameter) affects the unbalanced forces only by its internal load vector, so the unbalanced forces relation becomes $\mathbf{R}^{\mathrm{st}} = -\mathbf{R}_{\mathrm{int}}(\lambda_t^{st}) = \mathbf{0}$. Therefore, the equilibrium for each step is achieved when the thermal strains are internally balanced by the elastic strains for any element.

# 5 Numerical application

This presented formulation was implemented by the authors in an in-house FEM code and the following application allows to observe its capabilities. Figure 2 presents a two-dimensional representation of a slab subjected to variable thermal strains. This figure also shows the temperature field pattern for each step. This modelled slab is composed by plain concrete with its properties presented in Table 1. A slight fixed temperature gradient (from 0 ºC to 0.2 ºC) was applied along the slab height to induce the buckling within a stable path.

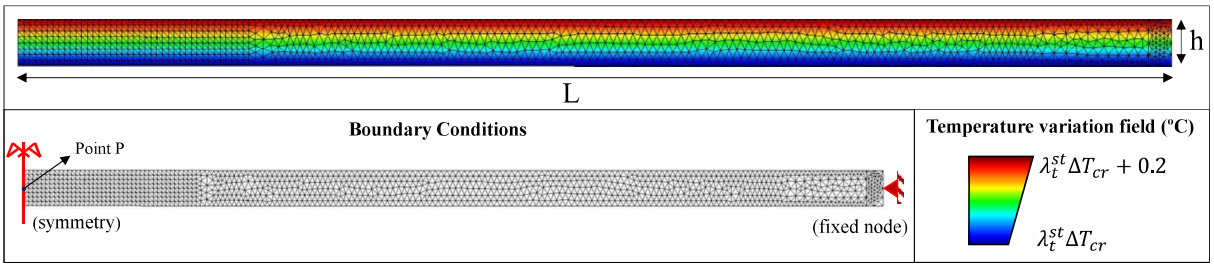


Figure 2. Plane-strain model of slab representation with temperature field and element discretization.

The temperature rising induces an elastic buckling due to compressive stresses. The critical temperature variation $\Delta T_{cr}$ can be evaluated as the one which induces an axial compressive stress equivalent to the obtained by an axial compressive critical load $P_{cr} = (\pi^2 \mathrm{E\,t\,h^3})/[\,12(1-\nu^2)\,l_e^2\,]$ for plane strains problems. The vertical displacements must increase after this temperature is reached, as flexural stresses arise and positives equivalent strains above $\mathcal{K}_0$ starts to appear at the top of the slab from the symmetry side. Naturally, the additional temperature gradient slightly diverts the obtained result (as represented by the red dotted temperature-deflection path in Graph 1) from the expected one to avoid the bifurcation point. Despite this, the observed result still shows the geometrically nonlinear nature of this transformation.

| **Geometry** | | **Thermo-mechanical properties** | | | | **Nonlocal Damage Parameters** | | | |
|---|---|---|---|---|---|---|---|---|---|
| Length L (m) | 5.0 | Young's Modulus E (MPa) | | | 3.0E+04 | $A_T$ | 0.9 | $\mathcal{K}_0$ | 3.0E-05 |
| Height h (m) | 0.2 | Poisson's ratio $\nu$ | | | 0.2 | $B_T$ | 1.0E+04 | $d_{lim}$ (cm) | 2.0 |
| Thickness t (m) | 1.0 | Thermal expansion coeff. $\alpha$ (1/°C) | | | 1.0E-05 | $A_C$ | 1.2 | | |
| Effective length $l_e$ (m) | 10.0 | $P_{cr}$ (N) | 2.06E+06 | $\Delta T_{cr}$ (°C) | 22.0 | $B_C$ | 1.5E+03 | | |

Table 1. Model geometry, thermo-mechanical properties and damage parameters for numerical application.

Graph 1 and Figure 3 present the main results. To avoid problems with unreal high strains in the fixed node, the region near this point was modelled to be insensitive to damage growth. The Graph 1 present the temperature-deflection curves at point P (from Figure 2) for undamaged simulation and both nonlocal and local damage approaches. Figure 3 presents the scalar damage field and the deflections for the nonlocal model, considering points A, B and C from Graph 1. Such points represent, respectively, the last converged step before the material instability (which is also the last step converged for the local analysis before the solution diverges, see green path in Graph 1), the first converged step after the instability (B) and a step in an already advanced state of damage over the entire length of the slab (C). The results evidence the nonlinear behavior induced by the slab buckling for both undamaged and damaged paths, while the physical nonlinearity induced by damage growth was better captured by the nonlocal damage. It should be observed a gap between consecutive steps A and B (gray dotted line) that must be related to an instable path (a vertical "jump" occurs between both solutions) that N-R procedure cannot capture (and an arc-length scheme may be demanded).

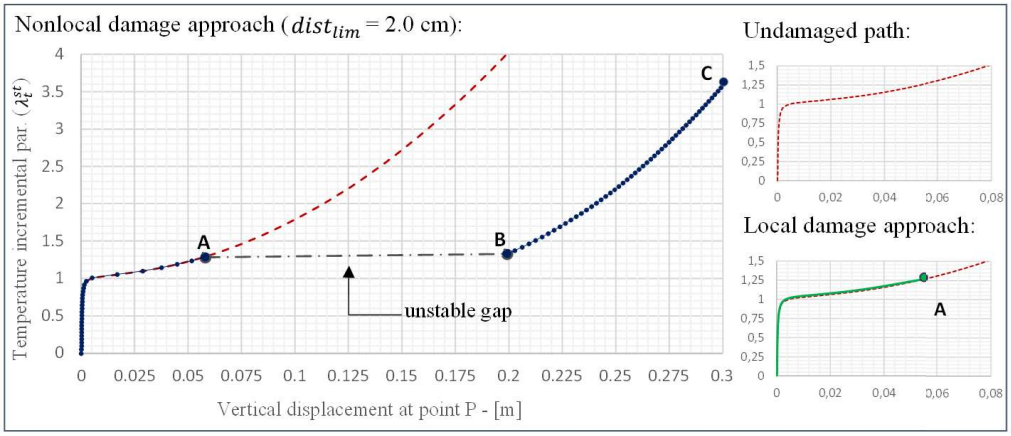


Graph 1. Temperature-deflection curves at point P for undamaged, local and nonlocal damage tests.

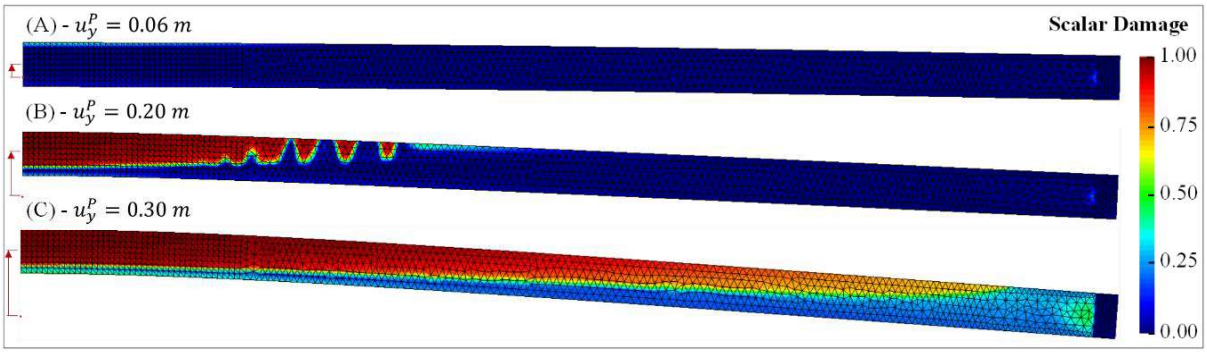


Figure 3. Scalar damage field and vertical slab deflection for temperature increase.

# 6 Conclusion

This work is a continuation from a former work by some of the authors presented in [4]. We found that the partial results presented here are promising in properly capturing the damage growth of the material, mainly when subjected to instabilities due to thermal strains. As a next step, we aim to incorporate a modified arc-length scheme within the solution method, with which we hope to be able to capture the unstable part of the load-deflection curve and also more complex behaviors regarding physical and geometric instabilities for different problems.

**Acknowledgements.** Second author acknowledges support by CNPq (Conselho Nacional de Desenvolvimento Científico e Tecnológico), Brazil, under the grant 307368/2018-1.

The authors hereby confirm that they are the sole liable persons responsible for the authorship of this work, and that all material that has been herein included as part of the present paper is either the property (and authorship) of the authors, or has the permission of the owners to be included here.

# References

[1] T. Belytschko, Z. P. Bažant, H. Yul-Woong, and C. Ta-Peng, "Strain-softening materials and finite-element solutions," *Comput. Struct.*, vol. 23, no. 2, pp. 163–180, 1986.

[2] Z. P. Bažant and G. Pijaudier-Cabot, "Nonlocal Continuum Damage, Localization Instability and Convergence," *J. Appl. Mech.*, vol. 55, no. 2, pp. 287–293, Jun. 1988.

[3] G. Pijaudier-Cabot and L. Jason, "Continuum Damage Modelling and Some Computational Issues," *Rev. Française Génie Civ.*, vol. 6, 2002.

[4] H. C. F. Curci, E. M. B. Campello, H. C. Gomes, and F. L. Maranhão, "Geometrically nonlinear limit point analysis of concrete structures with damage and temperature effects," in *Proceedings of the XL Ibero-Latin-American Congress on Computational Methods in Engineering - CILAMCE 2019*, 2019.

[5] S. C. H. Lu and K. S. Pister, "Decomposition of deformation and representation of the free energy function for isotropic thermoelastic solids," *Int. J. Solids Struct.*, vol. 11, no. 7, pp. 927–934, 1975.

[6] M. Micunovic, "A geometrical treatment of thermoelasticity of simple inhomogeneous bodies. I: Geometrical and kinematical relations," *Bull. l'Académie Pol. des Sci. Série des Sci. Tech.*, vol. 22, 1974.

[7] L. Vujošević and V. A. Lubarda, "Finite-strain thermoelasticity based on multiplicative decomposition of deformation gradient," *Theor. Appl. Mech.*, vol. 28, 2002.

[8] E. M. B. Campello, "Modelos não-lineares de casca em elasticidade e elastoplasticidade com grandes deformações: teoria e implementação em elementos finitos," Escola Politéccnica da Universidade de São Paulo, 2005.

[9] E. M. B. Campello, P. Pimenta, and P. Wriggers, "A triangular finite shell element based on a fully nonlinear shell formulation," *Comput. Mech.*, vol. 31, pp. 505–518, 2003.

[10] Eduardo W. V. Chaves, *Notes on Continuum Mechanics*. Springer, Dordrecht, 2013.

[11] P. Wriggers, *Nonlinear Finite Element Methods*. Springer, Berlin, Heidelberg, 2008.

[12] H. C. Gomes, "Método dos Elementos Finitos com Fronteiras imenras aplicado a problemas de dinâmica dos Fluidos e Interação Fluido Estrutura," Escola Politéccnica da Universidade de São Paulo, 2013.

[13] J. Mazars, "A description of micro- and macroscale damage of concrete structures," *Eng. Fract. Mech.*, vol. 25, no. 5, pp. 729–737, 1986.

[14] G. Pijaudier-Cabot and Z. Bazant, "Nonlocal Damage Theory," *J. Eng. Mech. - J ENG MECH-ASCE*, vol. 113, 1987.

[15] M. da Silva Alvares, "Estudo de um modelo de dano para o concreto: Formulação, identificação paramétrica e aplicação com o emprego do método dos elementos finitos," Escola de Engenharia de São Carlos, Universidade de São Paulo, 1993.